Journal of Inorganic and Organometallic Polymers and Materials (2022) 32:3117–3127
https://doi.org/10.1007/s10904-022-02345-6

Effect of Fe_2O_3 as an Aggregate Replacement on Mechanical, and Gamma/ Neutron Radiation Shielding Properties of Phosphoaluminate Glasses

A. A. El-Maaref[1] · B. M. Alotaibi[2] · Nuha Alharbi[3] · A. F. Abd El-Rehim[4,5] · Kh. S. Shaaban[6]

Received: 11 March 2022 / Accepted: 6 April 2022 / Published online: 28 April 2022
© The Author(s), under exclusive licence to Springer Science+Business Media, LLC, part of Springer Nature 2022

Abstract
In the present work, we examined the impact of Fe_2O_3 on the mechanical and photon shielding characteristics of lead-phosphoaluminate glasses. Due to water corrosion, the use of lead-phosphosilicate glasses may be limited.The addition of Fe_2O_3 significantly improves its water resistance. The radiation and mechanical of $20PbO - 45P_2O_5 - 15\ Al_2O_3 - (20 - x)\ Na_2O$- $x\ Fe_2O_3$glass system doped with xFe_2O_3reflect the originality of this article. The molar volume of these samples is declining whereas the density is an increment. Ultrasonic velocity and elastic modulus were found to be enhanced. The shielding parameters were established using the Phy-X / PSD. The mace attenuation coefficient is the highest in the sample with the maximum Fe_2O_3 content. The (Z_{eff}) and (N_{eff}) values decreased and then increased slowly at lower energy. Because of the Compton scattering interaction, the (Zeq)-value decreases as the energy and Fe_2O_3content increase. Small deviations from the glass samples are observed at higher energy levels to decrease the value (ΣR). Finally, the increment of Fe_2O_3 in prepared glasses increases the γ-radiation & neutronattenuation rate.

Keywords Phosphoaluminate · Elastic modulus · Shielding · Neutron

1 Introduction

Glass is an amorphous material that melts without crystallizing. High-manufacture phosphate glasses are used intended for numerous configurations [1–7]. The features of iron-phosphosilicate mixed glass networks are different from those of single glass networks [8–16]. There are several physical-chemical features of the transition metal ions (TMIs) doped phosphosilicate glasses that lead to a wide range of discussions of those samples in material knowledge. In detail, transition metal oxides (TMO) are widely perceived in phosphate glasses that are used to improve their chemical resistance. Fe_2O_3 and PbO are important elements because of their physical and mechanical characteristics. Fe_2O_3 and PbO glasses have specific characteristics as a result of their mechanical and radiation applications [17–24].

Iron alkaline phosphosilicate glasses have significant scientific and technological advancements. The structural benefits involved with the existence of PO_4 are responsible for this significance. Besides phosphate glass, the presence of TMIs, for example, Fe_2O_3 and PbO can provide new possibilities to extend these glasses' features. Heavy metal oxide doped glasses as PbO exhibition these glasses are highly optical, and mechanical because they act as a former and modifier. The presence of TMIs, such as Fe_2O_3 and PbO, in phosphosilicate glasses, can provide novel potentials for extending the features of these glasses [17–23].

✉ A. A. El-Maaref
aauelmaaref@ju.edu.sa

[1] Physics Department, College of Science, Jouf University, P.O. Box 2014, Skaka, Saudi Arabia

[2] Physics Department, College of Science, Princess Nourah bint Abdulrahman University, P.O. Box 84428, 11671 Riyadh, Saudi Arabia

[3] Physics Department, Faculty of Science, Umm Al-Qura University, Makkah, Saudi Arabia

[4] Physics Department, Faculty of Science, King Khalid University, P.O. Box 9004, 61413 Abha, Saudi Arabia

[5] Physics Department, Faculty of Education, Ain shams University, P.O. Box 5010, 11771 Heliopolis, Roxy, Cairo, Egypt

[6] Department of Chemistry, Faculty of Science, Al - Azhar University, P.O. 71452, Assiut, Egypt

Radiation has an incredible influence and has extremely large requests in our daily lives for everything we do. Radiation depletion can be used to determine the risk impacts on living organisms. As a result of its special properties in our lives, the application of radiation has enhanced, and the application of radiation shielding is increasing day by day. Many researchers used the glasses for various radiation protection [25–29].

The addition of Fe_2O_3 enhances the strength of the glass materials are used in gamma-ray shielding. Fe_2O_3 is commonly used in phosphate glasses to increase their chemical resistance to moisture attacks. Phosphate glasses containing alkali, alkaline earth metals and TMIs are having great importance as they are used as cathode materials in batteries. Among the various TMIs, the (Fe_2O_3) ions have a vigorous bearing on the innumerable properties particularly mechanical, optical and structural properties of glassy materials and which can exist in two different oxidations Fe^{2+} and Fe^{3+} states with different co-ordinations or environments. By keeping in view all the above methodologies, the radiation, and mechanical features of $20PbO - 45P_2O_5 - 15\ Al_2O_3 - (20-x)\ Na_2O$- xFe_2O_3 glass system doped with xFe_2O_3 reflect the originality of this article.

2 Materials and Methods

The melting and quenching process was used to synthesize iron-lead-phosphoaluminate glasses with a chemical formula of $45P_2O_5 - 15Al_2O_3 - 20PbO - (20-x)\ Na_2O$- $x\ Fe_2O_3$ ($0 \le x \le 2$) mol%. The mixture in the alumina crucible was preheated for 1 h in an electric furnace at 450 °C to remove moisture, CO_2, & NH_3. As a result, the melting process began right away in the same furnace, which was kept at 1150 °C for 1 h. The melted glass is quenched in a mould (inner size: Height 2 cm x thickness 1 cm x 1 cm) and annealed at 400 °C for 2 h to reduce internal thermal stress. Glass samples in Table 1 were prepared by traditional technique as the following equation: $Na_2CO_3 + Fe_2O_3 + PbO + Al_2O_3 + 2(NH_4)_2HPO_4 \xrightarrow[-(4NH3+6H2O+CO2)]{\Delta\ at\ 450\ ^\circ C} [Na_2O + Fe_2O_3 + PbO + P_2O_5 + Al_2O_3] \xrightarrow{\Delta 1150^\circ C}$ glasses $\xrightarrow{\text{annealing at } 400^\circ C}$ samples. The density is determined using Archimedes Code. Molar volume is established by $Vm = M/\rho$. The pulse-echo method was used to obtain longitudinal (v_L) and shear (v_T) ultrasonic velocities at room temperature. A digital ultrasonic flaw detector (KARL DEUTSCH Echograph model 1085) was used in conjunction with x-cut and y-cut transducers (KARL DEUTSCH) operating at a fundamental frequency of 4 MHz. The ultrasonic velocity measurement has a ±10 m/s uncertainty. Elastic moduli were determined as: longitudinal $L = \rho v_l^2$, transverse $G = \rho v_t^2$, Young's $Y = (1+\sigma)2G$,& bulk $K = L - \left(\frac{4}{3}\right)G$. Using the model in refs. [19, 21], it is possible to estimate the elastic moduli of the glasses based on packing density *Vi* and dissociation energy Gi : $Vi = \left(\frac{3\pi}{4}\right)N_A(m\mathrm{R_A}^3 + n\mathrm{R_O}^3)m^3.mol^{-1}$, $Gi = \left(\frac{1}{V_m}\right)\sum_i GiXi$. Longitudinal $L = K + \left(\frac{4}{3}\right)G$, transverse $G = 30 * \left(\frac{V_i^2 G_i}{V_i}\right)$ Young's $Y = 8.36 V_i G_i$, bulk $K = 10V_i^2 G_i$. Poisson's ratio $\sigma = \frac{1}{2}$ - $\left(\frac{1}{7.2^* Vi}\right)$. Impedance; $Z = v_L\rho$. Hardness; $\mathrm{H} = \frac{(1-2\sigma)\mathrm{Y}}{6(1+\sigma)}$. Debye: $\theta_D = \frac{h}{k}\left(\frac{9N_A}{4\pi V_m}\right)^{\frac{1}{3}} M_s$. Average velocities $M_s = \frac{1}{3}\left(\left(\frac{1}{v_l^3}\right) + \left(\frac{2}{v_t^3}\right)\right)^{-\frac{1}{3}}$. Packing density & Oxygen molar volume: $V_o = \left(\frac{M}{\rho}\right)\left(\frac{1}{\sum xini}\right)$, $OPD = \left(\frac{1000C}{Vm}\right)\left(\frac{Mol}{L}\right)$, Fractal bond connectivity (d)= $4(G/K)$. Phy-X / PSD, by Sakar et al. [29] can compute several shielding factors at (0 MeV-15 MeV). Beer-Lambert law as written in Eq in mathematical form: $\mu = -\frac{ln\frac{I}{I_o}}{x}$, Where μ represents the linear attenuation coefficient (cm^{-1}) I_0 and I, respectively, show unattenuated and attenuated photon intensities. Mass attenuation coefficient (MAC) was calculated as follows: $\left(\frac{\mu}{\rho}\right) = \sum_i w_i\left(\frac{\mu}{\rho}\right)_i$. Mean free path (MFP), tenth and half-value layer (TVL), (HVL) considered as $MEP = \left(\frac{1}{\mu}\right)$, (TVL) (HVL) are calculated by: $\mathrm{TVL} = \left(\frac{\ln 10}{\mu}\right), \mathrm{HVL} = \left(\frac{\ln 2}{\mu}\right)$. The effective atomic number (Z_{eff}) is predictable by $Z_{eff} = \left(\frac{\sigma_a}{\sigma_e}\right)$ where (σ_a) is the atomic cross-section, $\sigma_a = \sigma_m \frac{1}{\sum_i n_i} = \left(\frac{\mu}{\rho}\right)_{target} / N_A \sum_i \frac{w_i}{A_i}$, and σ_e is the electronic cross-section, $\sigma_e = \frac{1}{N}\sum_i \left(\frac{\mu}{\rho}\right)_i \frac{f_i w A_i}{z_i}$. Equivalent atomic number Z_{eq} is predictable by $Zeq = \frac{Z1(\log R2 - \log R) + Z2(\log R - \log R1)}{\log R2 - \log R1}$. Electron density ($N_{eff}$) is predictable by $\mathrm{N_{eff}} = \mathrm{N}\frac{\mathrm{Z_{eff}}}{\sum_i \mathrm{F_i A_i}}$. Effective removal cross-section (Σ_R), is predictable as: $\left(\frac{\Sigma_R}{\rho}\right) = \sum_i \mathrm{w_i}\left(\frac{\Sigma_R}{\rho}\right)_i$ and $\mathrm{R} = \sum_i \rho_i\left(\frac{\mathrm{R}}{\rho}\right)_i$

Table 1 The components of synthesized glasses

Code	Components (mol%)				
	P_2O_5	Al_2O_3	PbO	Na_2O	Fe_2O_3
G 1	45	15	20	20	0
G 2	45	15	20	19.5	0.5
G 3	45	15	20	19	1
G 4	45	15	20	18.5	1.5
G 5	45	15	20	18	2

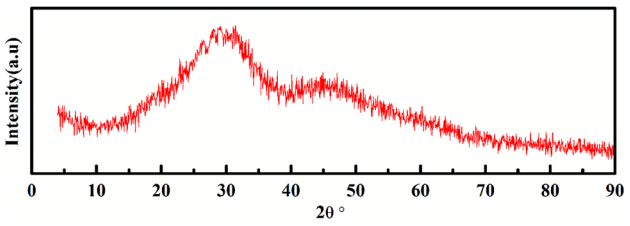

Fig. 1 XRD of G 3 synthesized glasses

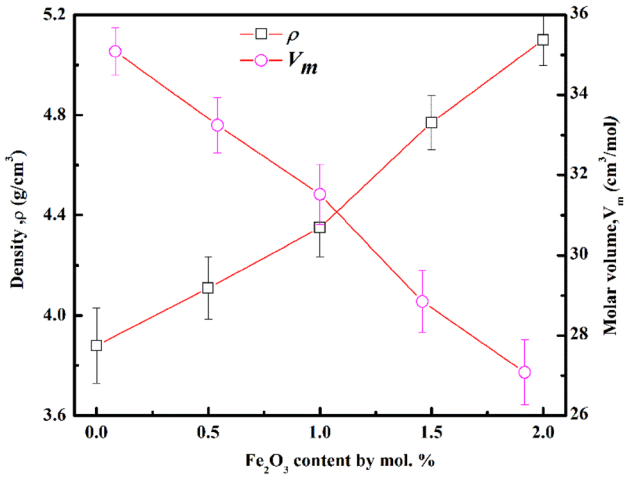

Fig. 2 ρ& V_m of prepared samples

Table 2 Various physical constraints

Samples	G 1	G 2	G 3	G 4	G 5
No	3.1	3.15	3.2	3.25	3.3
(N_i) (10^{21} ions/cm^3)	–	1.43	3	4.93	6.97
R_i (Å)	–	9.03	7.05	5.97	5.32
ri (Å)	–	10.45	8.17	6.94	6.19
r_p (Å)	–	3.00	2.35	1.99	1.78
(d_{P-P}) nm	0.55	0.53	0.52	0.50	0.48

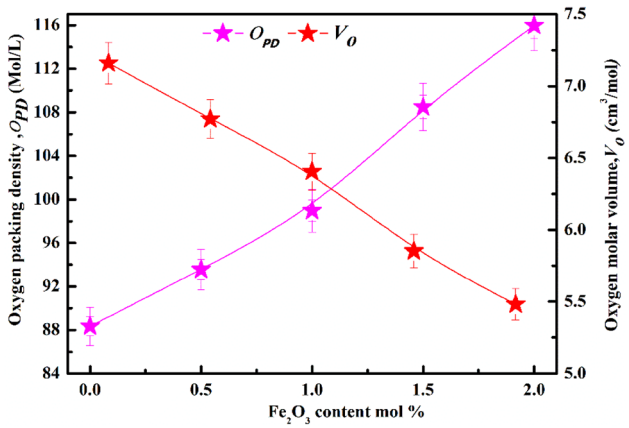

Fig. 3 V_o & OPD of prepared glasses

3 Results and Discussion

3.1 Physical Properties

The XRD of the glass system is illustrated in Fig. 1. the amorphous state of all glasses is detected. Figure 2 illustrates the molar volume (V_m) and glass density (ρ) as Fe_2O_3 concentration increases. The results demonstrate that ρ is increasing, while V_m decreases. Several factors, such as density and molecular mass, have a direct impact on the (ρ) and (V_m). The density of Na_2O and Fe_2O_3, (2.27, 5.25), and molecular weights (61.69, 159.688). The atomic radii of [Fe (0.83°A) & Na (1.8°A)] [30–35]. Fe-ions concentration was calculated as $Ni = \left(\frac{6.023\times10^{23}\,xmolfractionofcation\times valencyofcation}{Vm}\right)$. It is well-known that Fe^{3+}concentration increments due to the decreasing of V_m. Inter-ionic distance (R_i) calculated as $R_i = \left(\frac{1}{\text{contentofPb}}\right)^{\frac{1}{3}}$, it well-known that R_i declined, this decline is associated with reductions of V_m. P – P separation ($d_{P\text{-}P}$) could be estimated by $(dP-P) = \left(\frac{V_m^B}{N}\right)^{\frac{1}{3}}$ and $V_m^B = \frac{Vm}{2(1-2Xn)}$. The values of (dP – P) increased due to the decrease of V_m. Radius Polaron r_p & distance inter-nuclear r_i are predictable by $rp = \frac{1}{2}\left(\frac{\pi}{6N}\right)^{\frac{1}{3}}$, $ri = \left(\frac{1}{N}\right)^{\frac{1}{3}}$. It is mentioned that, with the increases of Fe^{3+} these values become smaller, due to reduction of V_m. Table 2 documents these estimations. The variations in V_o and OPD are exemplified in Fig. 3. The V_o values are decreased, while OPD increased.

3.2 Mechanical Properties

Figure 4 exemplifies the velocities ($v_{L,}$ v_T) of glasses. With an increase in Fe_2O_3 content, each velocity is increased and documented in Table 3 [36–43]. Arrange v_L between 5252, 5370 m/s and v_T 3067, 3136 m/s. When Fe_2O_3 is increased, the network glass modifier increases, explaining the observed variations in ($v_{L,}$ v_T) of the glasses. This oxide causes bond lengths to shorten and ultrasonic velocities to increase by increasing the stretching force constantly. Furthermore, the increased in v_L and v_T of the investigated glasses can be linked to the higher bond strength of Fe–O than Na–O.

Figures 5 and 6 show elastic moduli with Fe_2O_3 content (experimentally and theoretically). Elastic modulus values decreased with the reduction of Fe_2O_3 content. This behavior is attributed to an increment in coordination number as Fe_2O_3 rises, in addition to the increase in the average force and cross-link density. As Na_2O replaces Fe_2O_3, V_m reduces,

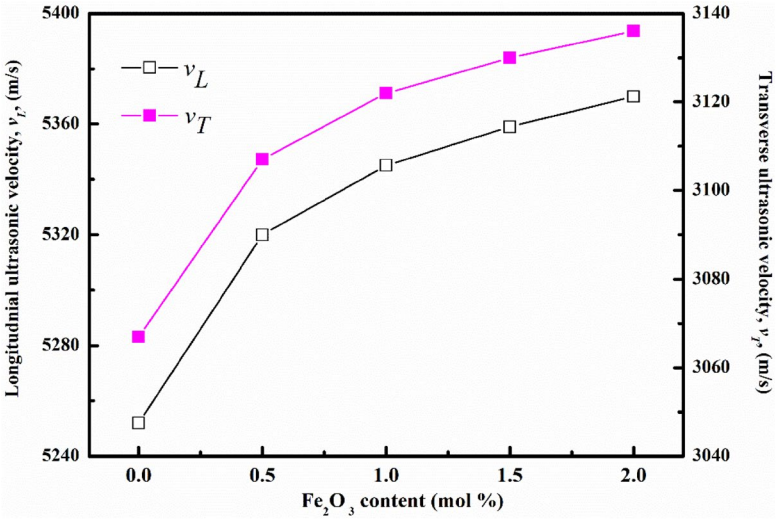

Fig. 4 (v_l&v_t) of synthesized glasses

and the ρ rises, attempting to make the glass matrices extra compact. The above results are listed in Table 3. This could be because the elastic moduli are dependent on the density values, which are increased when Fe_2O_3 is added to the glasses, compacting the glass structure, and increasing network rigidity.

Mechanical values (*Vi*), (*Gi*), (*H*), (α_P), (Z), (O_{PD}), (*Vo*), and (σ) are listed in Table 4. (*Vi*), (*H*), (α_P), (Z), (O_{PD}), (d), and (σ) is increased with Fe_2O_3, whereas (*Gi*) decrements. The content of the network modifier (NWM) is linked to an enhancement in the glass structure's rigidity. The addition of Fe_2O_3 also increased crosslink density and sample compactness due to the current glassy samples' small variability in configuration. The fractal bond connectivity (*d*) is an important parameter that connects the elastic properties of the glasses to their structures. The values of (*d*) around 3. The structure of the glassy samples will be converted into a 3D network as the Fe_2O_3 content increases.

3.3 Radiation Properties

In terms of γ- shielding, a lead phosphosilicate glass system doped with Fe_2O_3 has been explored [44–60]. The MAC of the glass under consideration is the first criterion to be explained. Figure 7 illustrates the MAC of the glasses and estimated by $\left(\frac{\mu}{\rho}\right) = \sum_i w_i \left(\frac{\mu}{\rho}\right)_i$.Table 5 presents values of MAC. The reducing order of the samples is (G1) > (G2) > (G3) > (G4) > (G5), because of the atomic number variance between Fe and Na, this is not a significant increase. It is demonstrated that the MAC of the glass system increased at low energy and then stayed constant at higher energy [32, 34, 36–38, 41–43]. MAC trend with energy is the same as observable and is monitored by the major procedures of common gamma-ray interaction as photoelectric (PE) effect, Compton effect (CE), and pair production (PP) effect. MAC of glasses under-investigated compared to other samples are presented in Table 6.

Figure 8 shows the Z_{eff} of studied samples with γ-energy. The glass with the code G1 possesses the maximum score, whereas G5 possesses the minimum. The trend order of the samples is (G1) *Zeff* > (G2) *Zeff* > (G3) *Zeff* > (G4) *Zeff* > (G5) *Zeff*. The obtained results for *Zeff* values are shown in Table 7. The rate of -radiation attenuation for the glasses is accelerated as a result of the addition of Fe_2O_3 to the glasses [32, 34, 36–38, 41–43]. Figure 9 represents the (N_{eff}) with energy. (N_{eff}) has the same behaviour as *Zeff* [44–60].

The (Zeq) values of prepared samples were represented in Fig. 10. It is illustrated that (Zeq) increased with energy and with the replacement of Na_2O with Fe_2O_3. The (Zeq) values are reduced with energy increased and with the Fe_2O_3 content because of the Compton scattering interaction. The highest (Zeq) value is 1 MeV for prepared samples. The obtained results for *Zeff* values are shown in Table 8 [44–60].

(TVL), and (HVL) of prepared samples are shown in Fig. 11,&12. The shielding capacity of glasses possessing lowering HVL is the greatest. In this regard, of all the synthesized glasses, G5 appeared to be the most effective at shielding against gamma ionizing radiation. The trend order of the samples is (G1) *HVL* > (G2) *HVL* > (G3) *HVL* > (G4) *HVL* > (G5) *HVL*. Table 9 summarises the HVL results. TVL& HVL possess the same trend as the synthesized samples [44–60].

Figure 13 depicts the change in MFP. MFP values increased as photon energy increased. Additionally, MFP decreased as Fe_2O_3 content increased. This information reveals that as the photon's energy increases, it becomes capable of transmitting the prepared sample on purpose. For the best attenuation capabilities, G5 glass is recommended.

Table 3 Mechanical parameters values

code	V_L (m/s)	V_T (m/s)	L (GPa)	G (GPa)	K (GPa)	Y (GPa)	L_M (GPa)	G_M (GPa)	K_M (GPa)	Y_M (GPa)
G 1	5252	3067	107.02	36.50	58.36	90.60	112.16	32.37	68.99	79.56
G 2	5320	3107	116.32	39.68	63.42	98.49	121.93	33.86	76.78	83.91
G 3	5345	3122	124.28	42.40	67.74	105.24	132.52	35.41	85.31	88.41
G 4	5359	3130	136.99	46.73	74.68	116.00	152.69	38.21	101.74	96.5
G 5	5370	3136	147.07	50.16	80.19	124.51	169.176	40.365	115.36	102.75

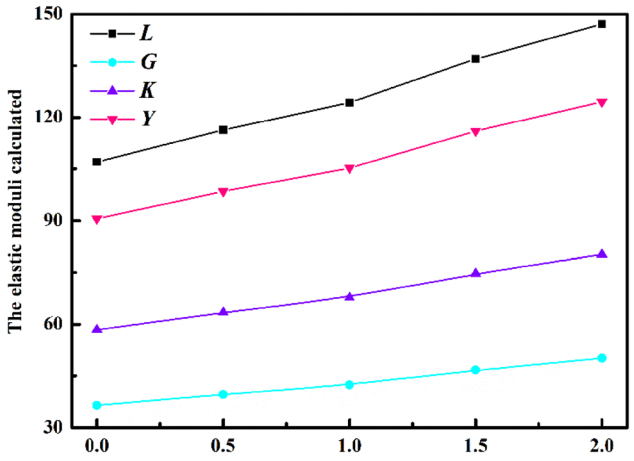

Fig. 5 $(L, G, K\&Y)$ of prepared glasses

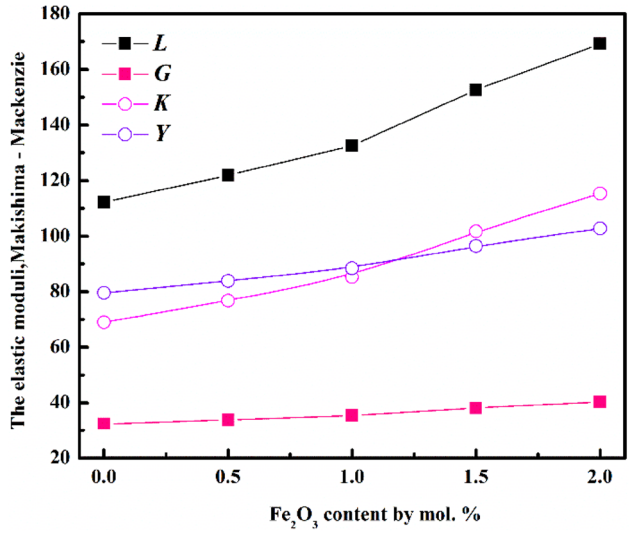

Fig. 6 $(L, G, K\&Y)$ of prepared glasses as calculated by Makishima and Mackenzie

It is well known that MEP and shielding have a relationship, with lower MFP values indicating better shielding material.

Figure 14 shows the (ΣR) of fabricated samples. At lower energy, it is detected that (ΣR) increment with energy. At higher energies, glass samples show minor deviations as (ΣR) decreases. Figure 15 depicts the Fast neutron removal cross-section (FNRCS).

of the glass system. It should be noted that as the Fe_2O_3 content increment, the FNRCS values increment [44–60]. In terms of FNRCS, the glasses are arranged in the following order: G5 > G4 > G3 > G2 > G1. The Fe_2O_3 content of the glasses supports this conclusion.

Table 4 Mechanical parameters values

Samples name/ parameters	$V_i x10^{-6}, (m^3)$	Gi, $(kcal/kJ)$	d	σ	$Zx10^7\ (kg.m^{-2}.s^{-1})$	θ_D, (K)	H, (GPa)	T_s, $(°C)$
G 1	0.73	13.13	2.5	0.241	2.04	434.37	6.30	1016.77
G 2	0.77	13.12	2.5	0.241	2.19	448.35	6.85	1045.09
G 3	0.81	13.11	2.5	0.241	2.32	458.90	7.32	1056.84
G 4	0.88	13.1	2.5	0.241	2.56	474.21	8.07	1063.89
G 5	0.94	13.1	2.5	0.241	2.74	485.61	8.65	1069.61

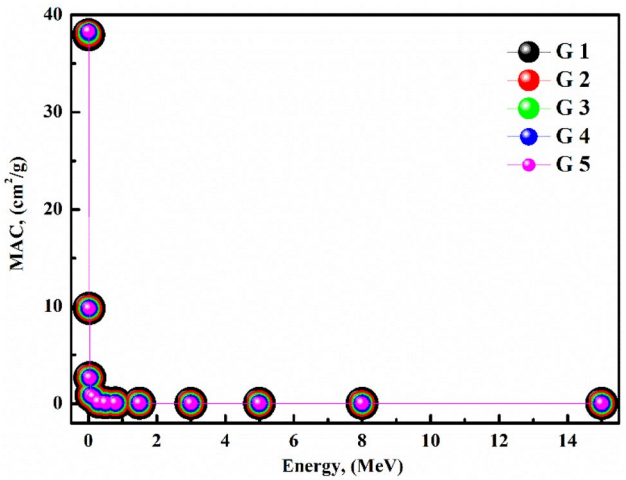

Fig. 7 MAC of prepared samples

Table 5 MAC of the glasses

Energy	G 1	G 2	G 3	G 4	G 5
0.015	37.940	38.032	38.123	38.213	38.303
0.02	28.033	28.036	28.038	28.040	28.042
0.03	9.825	9.823	9.820	9.818	9.815
0.04	4.689	4.687	4.685	4.682	4.680
0.05	2.666	2.664	2.662	2.661	2.659
0.06	1.700	1.699	1.697	1.696	1.695
0.08	0.869	0.868	0.867	0.867	0.866
0.1	1.804	1.799	1.794	1.789	1.784
0.15	0.709	0.707	0.705	0.704	0.702
0.2	0.390	0.389	0.388	0.387	0.386
0.3	0.196	0.196	0.196	0.195	0.195
0.4	0.136	0.136	0.136	0.136	0.136
0.5	0.109	0.109	0.109	0.109	0.109
0.6	0.093	0.093	0.093	0.093	0.093
0.8	0.076	0.076	0.075	0.075	0.075
1	0.065	0.065	0.065	0.065	0.065
1.5	0.051	0.051	0.051	0.051	0.051
2	0.045	0.045	0.045	0.045	0.045
3	0.038	0.038	0.038	0.038	0.038
4	0.034	0.034	0.034	0.034	0.034
5	0.033	0.033	0.033	0.033	0.033
6	0.032	0.032	0.032	0.032	0.032
8	0.031	0.031	0.031	0.031	0.031
10	0.031	0.031	0.031	0.031	0.031
15	0.032	0.032	0.032	0.032	0.032

4 Conclusions

The melt quenching procedure was used to manufacture a set of phosphate glasses with the following formulation:

Table 6 MAC (in cm^2/g) of prepared samples in assessment with diverse glasses

Samples	MAC, (MeV)	
	0.02	10
G 5 (Currently working)	28.042	0.031
$66B_2O_3$-$5Al_2O_3$-$29Na_2O$	1.074	0.020
$5Bi_2O_3$-$61B_2O_3$-$5Al_2O_3$-$29Na_2O$	5.059	0.022
$10Bi_2O_3$-$56B_2O_3$- $5Al_2O_3$-$29Na_2O$	9.043	0.023
0PbO-$30SiO_2$-$46.67B_2O_3$-$23.33Na_2O$	1.386	0.023
5PbO-$25SiO_2$-$46.67B_2O_3$-$23.33Na_2O$	5.167	0.021
10PbO-$20SiO_2$-$46.67B_2O_3$-$23.33Na_2O$	8.952	0.024
49.46SiO_2- 26.38Na_2O- 23.08CaO- 1.07P_2O_5	3.982	0.024
47.84SiO_2- 26.67Na_2O- 23.33CaO- 2.16P_2O_5	3.985	0.023
44.47SiO_2- 27.26Na_2O- 23.85CaO- 4.42P_2O_5	4.057	0.024
40.96SiO_2- 27.87Na_2O- 24.39CaO- 6.78P_2O_5	4.113	0.024
37.28SiO_2- 28.52Na_2O- 24.95CaO- 9.25P_2O_5	4.061	0.024
48.98SiO_2- 26.67Na_2O- 23.33CaO- 1.02P_2O_5	3.983	0.023
43.66SiO_2- 28.12Na_2O- 24.60CaO- 3.62P_2O_5	4.100	0.024
38.14SiO_2- 29.62Na_2O- 25.91CaO- 6.33P_2O_5	4.190	0.022
40.71SiO_2- 28.91Na_2O- 25.31CaO-5.07 P_2O_5	4.131	0.022

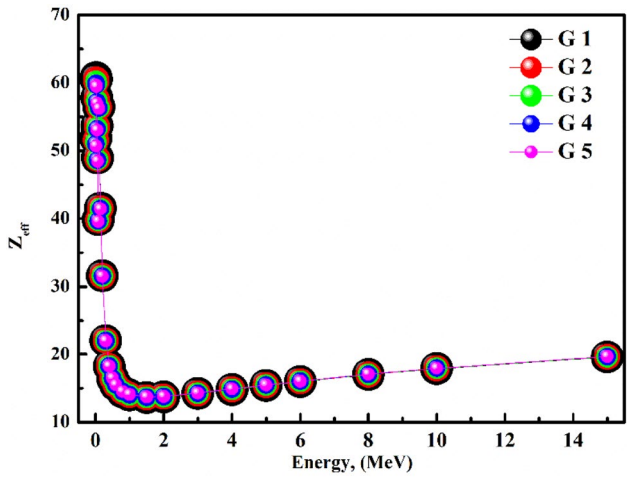

Fig. 8 (Z_{eff}) of prepared glasses

$x20PbO - 45P_2O_5 - 15Al_2O_3 - (20 - x)\ Na_2O$- $x\ Fe_2O_3$ ($0 \le x \le 2$).The mechanical and radiation characteristics of these glasses were examined. The density, ultrasonic velocity, and elastic moduli are incremented as the Fe_2O_3expands.Experimental results and calculated elastic moduli values using the Makishima-Mackenzie theoretical model are deemed acceptable. The parameters like MAC, LAC, TVL, HVL, MFP, and $\sum R$are computed to estimate the capabilities of glasses doped with Fe_2O_3 to shield radiation. The results show that as the Fe_2O_3 content increases, the values of $MAC$and $\sum R$ decrement.The G5 glass sample shields photons and neutrons better than

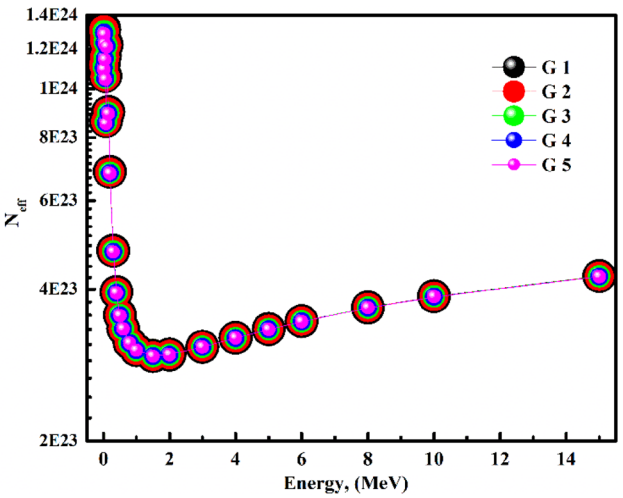

Fig. 9 (N_{eff}) of the synthesized samples

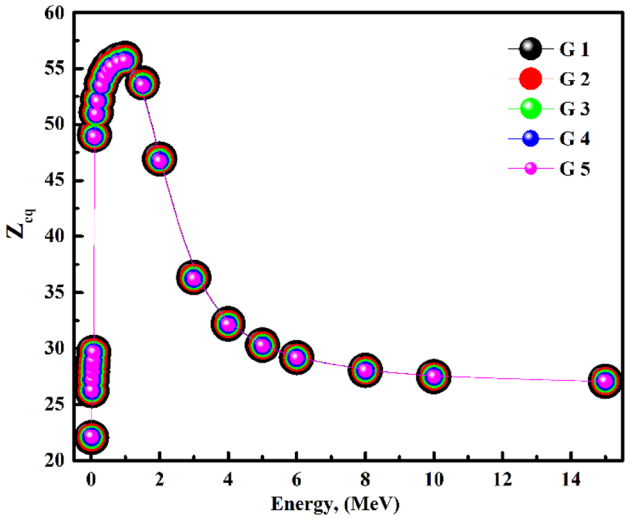

Fig. 10 (Zeq) of the synthesized samples

other glass samples, according to this investigation. The parameters' analysis revealed that the glasses under consideration are strong candidates for radiation shielding. Finally, the increase of Fe_2O_3 in prepared glasses increase γ-radiation attenuation rate.

Acknowledgements The authors express their gratitude to princess Nourah bint Abdulrahman University, Researchers Supporting Project (Grant No. PNURSP2022R32) Princess Nourah bint Abdulrahman University, Riyadh, Saudi Arabia. A.F. Abd El-Rehim extends his appreciation to the Deanship of Scientific Research at King Khalid

Table 7 Z_{eff} of the glasses

Energy	G 1	G 2	G 3	G 4	G 5
0.015	51.85	51.56	51.27	51.00	50.72
0.02	60.77	60.49	60.21	59.94	59.67
0.03	60.48	60.22	59.97	59.72	59.48
0.04	57.80	57.59	57.38	57.18	56.97
0.05	53.68	53.52	53.36	53.20	53.04
0.06	48.94	48.82	48.70	48.59	48.47
0.08	39.83	39.78	39.72	39.66	39.60
0.1	56.46	56.41	56.35	56.29	56.24
0.15	41.53	41.50	41.47	41.44	41.41
0.2	31.60	31.59	31.57	31.56	31.54
0.3	22.03	22.03	22.04	22.04	22.04
0.4	18.23	18.24	18.25	18.26	18.27
0.5	16.43	16.44	16.45	16.47	16.48
0.6	15.44	15.46	15.48	15.49	15.51
0.8	14.46	14.48	14.49	14.51	14.53
1	13.99	14.01	14.03	14.05	14.06
1.5	13.62	13.64	13.66	13.68	13.69
2	13.71	13.73	13.75	13.77	13.79
3	14.21	14.22	14.24	14.26	14.28
4	14.80	14.82	14.84	14.86	14.87
5	15.39	15.41	15.43	15.45	15.47
6	15.97	15.99	16.00	16.02	16.04
8	17.00	17.02	17.04	17.06	17.08
10	17.90	17.92	17.94	17.95	17.97
15	19.62	19.64	19.65	19.67	19.69

Table 8 *Zeq* of the glasses

Energy	G 1	G 2	G 3	G 4	G 5
0.015	22.07	22.09	22.11	22.13	22.15
0.02	26.25	26.25	26.25	26.25	26.25
0.03	27.23	27.23	27.23	27.23	27.23
0.04	27.94	27.94	27.93	27.93	27.93
0.05	28.50	28.49	28.49	28.48	28.47
0.06	28.95	28.94	28.93	28.93	28.92
0.08	29.69	29.68	29.67	29.66	29.65
0.1	49.04	48.99	48.95	48.90	48.85
0.15	51.07	51.02	50.97	50.92	50.87
0.2	52.24	52.19	52.13	52.08	52.03
0.3	53.63	53.58	53.52	53.47	53.42
0.4	54.45	54.40	54.35	54.29	54.24
0.5	54.99	54.94	54.88	54.83	54.78
0.6	55.35	55.29	55.24	55.19	55.14
0.8	55.74	55.68	55.63	55.58	55.52
1	55.90	55.84	55.79	55.74	55.68
1.5	53.70	53.65	53.59	53.54	53.49
2	46.91	46.86	46.81	46.75	46.70
3	36.34	36.31	36.28	36.24	36.21
4	32.22	32.20	32.18	32.16	32.14
5	30.30	30.29	30.28	30.27	30.25
6	29.20	29.19	29.18	29.17	29.16
8	28.05	28.05	28.04	28.04	28.04
10	27.50	27.50	27.50	27.50	27.49
15	27.08	27.08	27.08	27.08	27.08

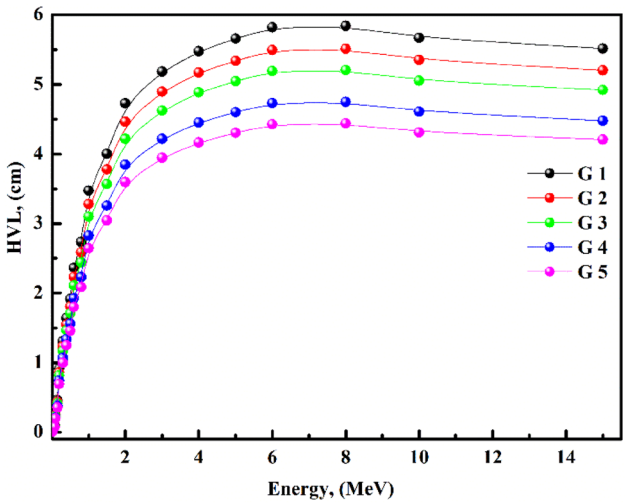

Fig. 11 HVL of the synthesized samples

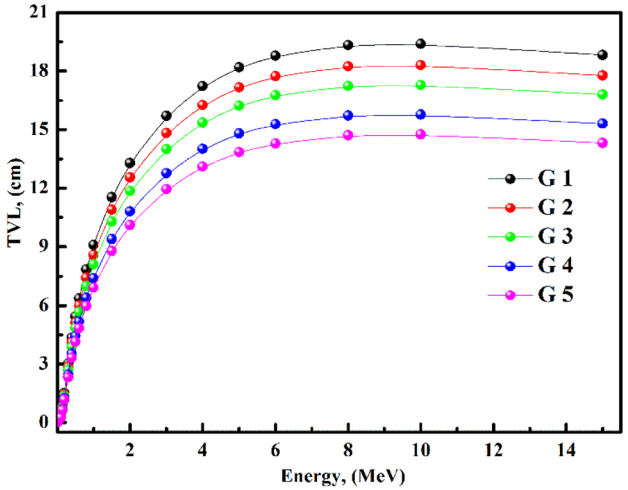

Fig. 12 TVL of the synthesized samples

Table 9 *HVL* of the glasses

Energy	G 1	G 2	G 3	G 4	G 5
0.015	0.005	0.004	0.004	0.004	0.004
0.02	0.006	0.006	0.006	0.005	0.005
0.03	0.018	0.017	0.016	0.015	0.014
0.04	0.038	0.036	0.034	0.031	0.029
0.05	0.067	0.063	0.060	0.055	0.051
0.06	0.105	0.099	0.094	0.086	0.080
0.08	0.206	0.194	0.184	0.168	0.157
0.1	0.099	0.094	0.089	0.081	0.076
0.15	0.252	0.238	0.226	0.207	0.194
0.2	0.458	0.434	0.411	0.375	0.352
0.3	0.910	0.860	0.814	0.743	0.696
0.4	1.310	1.238	1.171	1.069	1.001
0.5	1.639	1.549	1.465	1.337	1.251
0.6	1.915	1.809	1.710	1.561	1.460
0.8	2.365	2.234	2.111	1.926	1.802
1	2.739	2.586	2.444	2.229	2.086
1.5	3.475	3.281	3.100	2.828	2.645
2	4.002	3.779	3.571	3.257	3.046
3	4.728	4.464	4.218	3.847	3.598
4	5.186	4.896	4.626	4.219	3.947
5	5.477	5.170	4.885	4.455	4.167
6	5.657	5.340	5.046	4.602	4.304
8	5.819	5.493	5.190	4.733	4.427
10	5.837	5.511	5.207	4.748	4.441
15	5.669	5.351	5.056	4.610	4.312

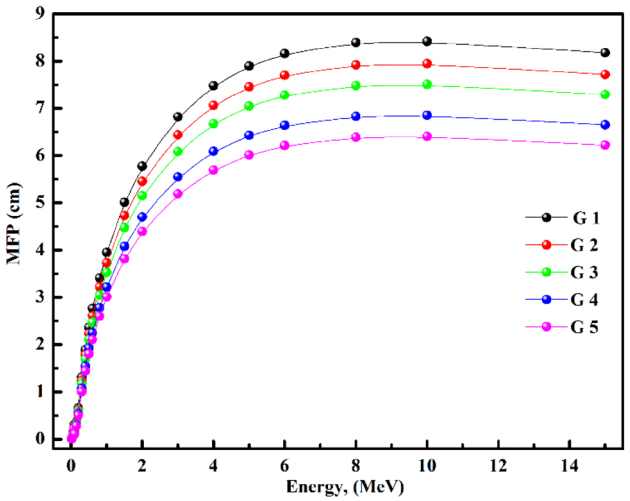

Fig. 13 MFP of the synthesized samples

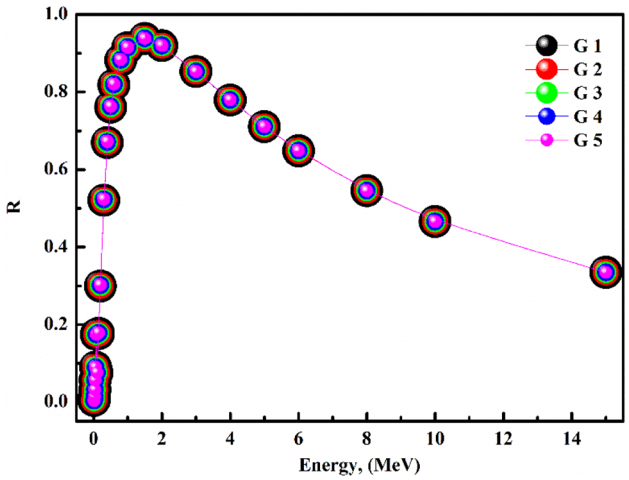

Fig. 14 (ΣR) of the synthesized samples

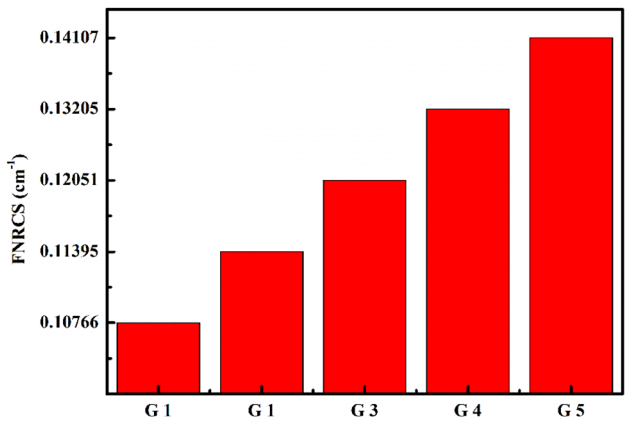

Fig. 15 FNRCS of the synthesized samples

University for funding this work through a research groups program under grant number R.G.P. 1/277/42.

Author Contributions All of the authors have taken full responsibility for the content of this manuscript.

Funding Not applicable.

Availability of Data and Material My manuscript and associated personal data.

Declarations

Conflict of interest The authors declare that they have no conflict of interest.

Compliance with Ethical Standards The manuscript has not been published elsewhere.

Declaration of Competing Interest There are no known competing financial interests among the authors.

Consent to Participate The author's consent to participate & publication.

References

1. A.M. Abdelghany, H.A. ElBatal, J. Mol. Struct. (2014) doi:https://doi.org/10.1016/j.molstruc.2014.03.032
2. A.M. Abdelghany, G. El-Damrawi, A.H. Oraby, M.A. Madshal, J. Non-cryst. Solids (2018) doi:https://doi.org/10.1016/j.jnoncrysol.2018.07.022
3. H.A. ElBatal, A.M. Abdelghany, F.H. ElBatal, K. ElBadry, F.A. Moustaffa, Phys. B: Condens. Matter (2011) doi:https://doi.org/10.1016/j.physb.2011.06.074
4. A.F.A. El-Rehim, A.M. Ali, H.Y. Zahran, I.S. Yahia, K.S. Shaaban, J. Inorg. Organomet. Polym. (2021) doi:https://doi.org/10.1007/s10904-020-01799-w
5. Y.B. Saddeek, K.A. Aly, K.S. Shaaban, A.M. Ali, M.M. Alqhtani, A.M. Alshehri, M.A. Sayed, E.A. Abdel, Wahab, J. Non-cryst. Solids (2018) doi:https://doi.org/10.1016/j.jnoncrysol.2018.06.002
6. K.S. Shaaban, Y.B. Saddeek, Silicon (2017) doi:https://doi.org/10.1007/s12633-017-9558-5
7. E.A.A. Wahab, A.M. Al-Baradi, M.A. Sayed, A.M. Ali, S.A. Makhlouf, K.S. Shaaban, Silicon (2022) doi:https://doi.org/10.1007/s12633-021-01652-w
8. E.A. Abdel Wahab, A.A. El-Maaref, K. Shaaban, J. Börcsök, M. Abdelawwad, Opt. Mater. (2021) doi:https://doi.org/10.1016/j.optmat.2020.110638
9. A.A. El-Maaref, S. Badr, K. Shaaban, E.A. Abdel Wahab, M.M. ElOkr, J. Rare Earths (2019) doi:https://doi.org/10.1016/j.jre.2018.06.006
10. A.M. Fayad, K.S. Shaaban, W.M. Abd-Allah, M. Ouis, J. Inorg. Organomet. Polym. (2020) doi:https://doi.org/10.1007/s10904-020-01641-3
11. K.S. Shaaban, A.M. Al-Baradi, A.M. Ali, Silicon (2022) doi:https://doi.org/10.1007/s12633-022-01702-x
12. K.S. Shaaban, Z.A. Alrowaili, A.M. Al-Baradi, A.M. Ali, E.A.A. Wahab, M.S. Al-Buriahi, Silicon (2021) doi:https://doi.org/10.1007/s12633-021-01441-5
13. K.S. Shaaban, E.A.A. Wahab, E.R. Shaaban, E.S. Yousef, S.A. Mahmoud, Opt. Quant. Electron. (2020) doi:https://doi.org/10.1007/s11082-020-2191-3
14. K.S. Shaaban, E.S. Yousef, S.A. Mahmoud, E.A.A. Wahab, E.R. Shaaban, J. Inorg. Organomet. Polym. (2020) doi:https://doi.org/10.1007/s10904-020-01574-x
15. K.S. Shaaban, H.Y. Zahran, I.S. Yahia, H.I. Elsaeedy, E.R. Shaaban, S.A. Makhlouf, E.A.A. Wahab, E.S. Yousef, Appl. Phys. A (2020) doi:https://doi.org/10.1007/s00339-020-03982-9
16. N. Sharmin, F. Gu, I. Ahmed, A.J. Parsons, J. tissue Eng. (2017) doi:https://doi.org/10.1177/2041731417744454
17. A.H. Almuqrin, K.A. Mahmoud, E.A.A. Wahab, M.S.I. Koubisy, M.I. Sayyed, K.S. Shaaban, Eur. Phys. J. Plus (2021) doi:https://doi.org/10.1140/epjp/s13360-021-01564-z
18. S. Alomairy, M.S. Al-Buriahi, E.A. Abdel Wahab, C. Sriwunkum, K. Shaaban, Ceram. Int. (2021) doi:https://doi.org/10.1016/j.ceramint.2021.03.045
19. A. El-Taher, A.M. Ali, Y.B. Saddeek, R. Elsaman, H. Algarni, K. Shaaban, T.Z. Amer, Radiat. Phys. Chem. (2019) doi:https://doi.org/10.1016/j.radphyschem.2019.108403
20. M.A. Sayed, A.M. Ali, A.F. Abd El-Rehim, E.A. Abdel Wahab, K.S. Shaaban, J. Elec Materi (2021) doi:https://doi.org/10.1007/s11664-021-08921-9
21. K.S. Shaaban, E.S. Yousef, E.A. Abdel Wahab, E.R. Shaaban, S.A. Mahmoud, J. of Materi Eng. and Perform. (2020) doi:https://doi.org/10.1007/s11665-020-04969-6
22. H.H. Somaily, K.S. Shaaban, S.A. Makhlouf, H. Algarni, H.H. Hegazy, E.A.A. Wahab, E.R. Shaaban, J. Inorg. Organomet. Polym. (2021) doi:https://doi.org/10.1007/s10904-020-01650-2
23. E.A. Abdel Wahab, K.S. Shaaban, S. Alomairy, M.S. Al-Buriahi, Eur. Phys. J. Plus (2021) doi:https://doi.org/10.1140/epjp/s13360-021-01572-z
24. P. Das, S. Ganguly, M. Bose, D. Ray, S. Ghosh, S. Mondal, V.K. Aswal, A.K. Das, S. Banerjee, N.C. Das, New. J. Chem. (2019) doi:https://doi.org/10.1039/c8nj06308g
25. E.A. Abdel Wahab, K.S. Shaaban, Appl. Phys. A (2021) doi:https://doi.org/10.1007/s00339-021-05062-y
26. B. Albarzan, A.H. Almuqrin, M.S. Koubisy, E.A. Wahab, K.A. Mahmoud, K. Shaaban, M.I. Sayyed, Prog. Nucl. Energy (2021) doi:https://doi.org/10.1016/j.pnucene.2021.103931
27. M.S. Al-Buriahi, Z.A. Alrowaili, I. Kebaili, A.M. Al-Baradi, E.A.A. Wahab, I.O. Olarinoye, C. Sriwunkum, K.S. Shaaban, Phys. Scr. (2021) doi:https://doi.org/10.1088/1402-4896/ac4121
28. K.S. Shaaban, A.M. Al-Baradi, Z.A. Alrowaili, A.M. Ali, M.S. Al-Buriahi, E.A.A. Wahab, J. Mater. Sci: Mater. Electron. (2021) doi:https://doi.org/10.1007/s10854-021-07158-w
29. K.S. Shaaban, S. Alomairy, M.S. Al-Buriahi, J. Mater. Sci: Mater. Electron. (2021) doi:https://doi.org/10.1007/s10854-021-05885-8
30. A.A. El-Maaref, R.M. El-Agmy, K.S. Shaaban, E.A. Abdel, Wahab, Eur. Phys. J. Plus (2021) doi:https://doi.org/10.1140/epjp/s13360-021-01798-x
31. A.A. El-Maaref, E.A. Wahab, K.S. Shaaban, R.M. El-Agmy, Solid State Sci. (2021) doi:https://doi.org/10.1016/j.solidstatesciences.2021.106539
32. A.F.A. El-Rehim, K.S. Shaaban, H.Y. Zahran, I.S. Yahia, A.M. Ali, M.M.A. Halaka, S.A. Makhlouf, E.A.A. Wahab, E.R. Shaaban, J. Inorg. Organomet. Polym. (2021) doi:https://doi.org/10.1007/s10904-020-01708-1
33. K.S. Shaaban, S.M. Abo-naf, A.M. Abd Elnaeim, M.E.M. Hassouna, Appl. Phys. A (2017) doi:https://doi.org/10.1007/s00339-017-1052-9
34. K. Shaaban, E.S. Yousef, Optik (2020) doi:https://doi.org/10.1016/j.ijleo.2019.163976
35. E.A.A. Wahab, A.M. Aboraia, A.M.E. Shafey, K.S. Shaaban, A.V. Soldatov, Opt. Quant. Electron. (2021) doi:https://doi.org/10.1007/s11082-021-03164-8
36. M.A. Azooz, Y.B. Saddeek, K.A. Aly, K.S. Shaaban, H.M. Mokhtar, J. Inorg. Organomet. Polym. (2019) doi:https://doi.org/10.1007/s10904-019-01130-2
37. Y.B. Saddeek, K.A. Aly, K.S. Shaaban, A.M. Ali, M.A. Sayed, Silicon (2019) doi:https://doi.org/10.1007/s12633-018-9912-2
38. K. Shaaban, Y.B. Saddeek, K. Aly, Ceram. Int. (2018) doi:https://doi.org/10.1016/j.ceramint.2017.11.175
39. K.S. Shaaban, S.M. Abo-naf, M.E.M. Hassouna, K.S. Shaaban, S.M. Abo-naf, Silicon (2019) doi:https://doi.org/10.1007/s12633-016-9519-4
40. K.S. Shaaban, A.M. Ali, Y.B. Saddeek, K.A. Aly, A. Dahshan, S.A. Amin, Silicon (2019) doi:https://doi.org/10.1007/s12633-018-0004-0
41. K.S. Shaaban, Y.B. Saddeek, M.A. Sayed, I.S. Yahia, K.S. Shaaban, Silicon (2018) doi:https://doi.org/10.1007/s12633-017-9709-8

42. K.S. Shaaban, M.A. Sayed, Y.B. Saddeek, I.S. Yahia, K.S. Shaaban, Silicon (2019) doi:https://doi.org/10.1007/s12633-016-9465-1
43. E.A.A. Wahab, K.S. Shaaban, Mater. Res. Express (2018) doi:https://doi.org/10.1088/2053-1591/aaaee8
44. E.A. Abdel Wahab, M. Koubisy, M.I. Sayyed, K.A. Mahmoud, A.F. Zatsepin, S.A. Makhlouf, K. Shaaban, J. Non-cryst. Solids (2021) doi:https://doi.org/10.1016/j.jnoncrysol.2020.120509
45. A.S. Abouhaswa, M.I. Sayyed, A.S. Altowyan, Y. Al-Hadeethi, K.A. Mahmoud, Opt. Mater. (2020) doi:https://doi.org/10.1016/j.optmat.2020.109981
46. A.S. Abouhaswa, M.I. Sayyed, A.S. Altowyan, Y. Al-Hadeethi, K.A. Mahmoud, J. Non-cryst. Solids (2020) doi:https://doi.org/10.1016/j.jnoncrysol.2020.120134
47. A.M. Al-Baradi, A.F.A. El-Rehim, Z.A. Alrowaili, M.S. Al-Buriahi, K.S. Shaaban, Silicon (2021) doi:https://doi.org/10.1007/s12633-021-01481-x
48. S. Alomairy, A.M. Aboraia, E.R. Shaaban, K.S. Shaaban, Braz J. Phys. (2021) doi:https://doi.org/10.1007/s13538-021-00928-1
49. M.A. Alothman, Z.A. Alrowaili, J.S. Alzahrani, E.A. Wahab, I.O. Olarinoye, C. Sriwunkum, K. Shaaban, M.S. Al-Buriahi, J. Alloys Compd. (2021) doi:https://doi.org/10.1016/j.jallcom.2021.160625
50. Z.A. Alrowaili, A.M. Al-Baradi, M.A. Sayed, A. Mossad Ali, E.A. Abdel Wahab, M.S. Al-Buriahi, K. Shaaban, Optik (2022) doi:https://doi.org/10.1016/j.ijleo.2021.168259
51. Z.A. Alrowaili, A.M. Ali, A.M. Al-Baradi, M.S. Al-Buriahi, E.A.A. Wahab, K.S. Shaaban, Opt. Quant. Electron. (2022) doi:https://doi.org/10.1007/s11082-021-03447-0
52. A.A. El-Rehim, H.Y. Zahran, I.S. Yahia, S.A. Makhlouf, K.S. Shaaban, Silicon (2021) doi:https://doi.org/10.1007/s12633-020-00798-3
53. A.F.A. El-Rehim, K.S. Shaaban, J. Mater. Sci: Mater. Electron. (2021) doi:https://doi.org/10.1007/s10854-020-05204-7
54. A.F.A. El-Rehim, H.Y. Zahran, I.S. Yahia, A.M. Ali, K.S. Shaaban, Silicon (2022) doi:https://doi.org/10.1007/s12633-020-00827-1
55. M.S.I. Koubisy, K.S. Shaaban, E.A.A. Wahab, M.I. Sayyed, K.A. Mahmoud, Eur. Phys. J. Plus (2021) doi:https://doi.org/10.1140/epjp/s13360-021-01125-4
56. Y.S. Rammah, F.I. El-Agawany, K.A. Mahmoud, R. El-Mallawany, E. Ilik, G. Kilic, J. Mater. Sci: Mater. Electron. (2020) doi:https://doi.org/10.1007/s10854-020-03440-5
57. Y.S. Rammah, F.I. El-Agawany, E.A. Wahab, M.M. Hessien, K. Shaaban, Radiat. Phys. Chem. (2022) doi:https://doi.org/10.1016/j.radphyschem.2021.109956
58. Y.S. Rammah, K.A. Mahmoud, E. Kavaz, A. Kumar, F.I. El-Agawany, Ceram. Int. (2020) doi:https://doi.org/10.1016/j.ceramint.2020.04.018
59. Y.B. Saddeek, K. Shaaban, R. Elsaman, A. El-Taher, T.Z. Amer, Radiat. Phys. Chem. (2018) doi:https://doi.org/10.1016/j.radphyschem.2018.04.028
60. K.S. Shaaban, A.M. Al-Baradi, A.M. Ali, J. Mater. Sci: Mater. Electron. (2022) doi:https://doi.org/10.1007/s10854-021-07530-w

Publisher's note Springer Nature remains neutral with regard to jurisdictional claims in published maps and institutional affiliations.